Human umbilical cord mesenchymal stem cell-derived exosomes alleviate neuronal damage in a rat model of Parkinson's disease by inhibiting microglia-mediated pyroptosis

Zhong-Xia Zhang
the First Hospital of Hebei Medical University
Wei Zhao
Hebei University of Chinese Medicine
Ping Gu
the First Hospital of Hebei Medical University
Yong-Jie Zhou
Hebei University of Chinese Medicine
Ruo-Yu Wu
Hebei University of Chinese Medicine
Lu-Yang Zhou
Hebei University of Chinese Medicine
Qing-Zhuo Cui
Hebei University of Chinese Medicine
Hong-Xu Chen
Hebei University of Chinese Medicine
Lin-Qi Zhang
Hebei University of Chinese Medicine
Ke Zhang
Hebei University of Chinese Medicine
Hong-Jun Xu
Hebei University of Chinese Medicine
Xi-Qing Chai
the First Hospital of Hebei Medical University
Sheng-Jun An (sjsjan@126.com)
Hebei University of Chinese Medicine
Shao-Kang Sun
Hebei University of Chinese Medicine

Article

Keywords: mesenchymal stem cells, exosomes, Parkinson's Disease, pyroptosis, neuroinflammation

Posted Date: May 27th, 2022

DOI: https://doi.org/10.21203/rs.3.rs-1663711/v1

Abstract

Parkinson's disease (PD) is a neurodegenerative disease characterized by dyskinesia and related to microglia-mediated pyroptosis. Stem cell-derived exosomes have small size, low immunogenicity, and the ability of transferring the effective substances of stem cells freely. In this study, exosomes were isolated from human umbilical cord mesenchymal stem cells (hucMSCs) and injected into PD rats induced by 6-hydroxydopamine (6-OHDA). We found that the exosomes were absorbed by dopaminergic neurons and microglia in the affected side and exosome treatment inhibited microglia activation and prevented nigral-striatal dopamine neuron damage. Furthermore, pretreatment cultured BV2 cells with exosomes inhibited TLR4/NF-κB/NLRP3 inflammasome induced by LPS/ATP. Therefore, exosomes inhibited pyroptosis and reduced the secretion of supernatant IL-1β and IL-18, improved the survival rate of SH-SY5Y. In addition, the potential targets of hucMSCs- exosomes treatment of PD was further identified by miRNA high throughput sequencing and protein spectrum sequencing.

Introduction

Parkinson's disease (PD) is a neurodegenerative disease with clinical manifestations of static tremor, bradykinesia, myotonia and abnormalities of posture and gait. The main pathological changes in PD are the degenerative death of dopaminergic neurons in the substantia nigra (SN) and a decrease in dopamine (DA) content in the striatum. Since McGeer et al. first observed microglia activation in the SN and basal ganglia in autopsy specimen of PD patients in 1988[1], many studies on autopsy, brain imaging and fluid biomarker have suggested that microglia-mediated neuroinflammation plays an important role in pathogenesis and progression of PD.

HucMSCs, one of the mesenchymal stem cells with sufficient source and low immunogenicity, improve the behavioral performance of PD animal models and the clinical symptoms of PD patients[2, 3]. However, they have limitations in maintaining activity, effective substance quantification and the blood-brain barrier penetration. Exosomes are nanoscale objects with the small diameter (30–150 nm) extracellular vesicles with double-layer membrane structure containing various miRNAs and proteins. These genes and proteins are able to fuse with the cell membrane of recipient cells, which becomes an advantageous treatment[4]. In our previous study, hucMSCs exosomes were transplanted into PD rat model through tail vein for the first time and showed a protective effect on the PD rats, and the mechanism was related to inhibiting neuronal apoptosis and enhancing autophagy [5].

Pyroptosis is a newly found programmed cell death which is based on the Gasdermin protein family with pore-forming effect and its mechanism is different from apoptosis and autophagy. Animal studies and clinical data suggest that PD is closely related to NLRP3 and NLRP3-mediated pyroptosis. It has been reported that hucMSCs- exosomes reduces liver damage[6] and retinitis in diabetic rats[7] through inhibiting NLRP3, and alleviates ischemic damage[8] by inhibiting pyroptosis. However, if hucMSCs- exosomes improve PD by inhibiting microglia-mediated pyroptosis remains unknown. Therefore, this study aims to

determine if hucMSCs- exosomes have beneficiary effects on PD model and explores if their neuroprotective effect is correlated to microglia activation and microglia-mediated pyroptosis.

Results

Typical characteristics of hucMSCs and hucMSCs- exosomes

To verify the characteristics of mesenchymal stem cells, we determined the morphology, cell growth curve revealed by trypan blue staining, and the surface markers by flow cytometry. The cells grew in parallel or spiring shape under microscope (Fig.1a). The cells displayed a subsequent logarithmic and platform growth period, which was in line with the growth of stem cells (Fig. 1b). The values of special cell surface antigens for MSCs CD73, CD105 and CD90 were greater than 99.9%, while the expressions of hematopoietic stem cell antigens CD34, CD45 and human leukocyte antigen (HLA)-DR were lesser than 0.5% (Fig. 1c). Red calcium deposition was observed during osteogenic induction. A large number of the oil red O positive lipid droplets were observed during adipogenesis induction, and the deposition of acid mucopolysaccharide with positive alisin blue staining was observed during chondrogenesis induction (Fig. 1d).

To identify exosome isolated from MSCs, transmission electron microscope, NTA and Western blot were used to detect the morphology, particle size and surface markers. We found that the extracted exosomes had a cup-shaped, cupholder-shaped or biconcave discoid-shaped double-layer membrane structure (Fig. 1e, left panel). The isolated particles with an average size of 131.7 nm peaked at 110.1 nm were accounted for 98.1% of the total particles, suggesting that the size of isolated particles was within the range of exosomes particle size (30-150nm) (Fig. 1e, middle). The expressions of exosome markers CD63, TSG101 and Alix were positive, while the expression of organelle protein Calnexin was negative (Fig. 1e, right).

Systemic administration of exosomes improved the motor function in PD rats

To prove the effect of exosomes on the behavior of PD model induced by 6-OHDA fixed-point injection, the apomorphine (APO)-induced rotation was selected at weeks 2, 4, 6, 8 after transplantation (Fig. 2a). Compared with the 6-OHDA group, the rotational numbers in exosomes-lateral ventricle group decreased significantly from week 6 and in exosomes-tail vein group decreased significantly from week 4 after exosome injection (Fig. 2b, $P<0.01$). In order to observe whether the exosomes can cross the BBB, PKH-26-labeled exosomes were injected into tail vein and lateral ventricle in PD model for 24h. We found that exosomes were co-located with the damaged DA neuron (Fig. 2c) and microglia (Fig. 2d) in the lesioned substantia nigra.

We then used high-performance liquid chromatography-mass spectrometric (HPLC-MS) to detect the content of 5-HT, its metabolites 5-HIAA, DA, and DA's metabolites DOPAC and HVA in the striatum. Compared with 6-OHDA group, the contents of DA, 5-HIAA ($P<0.01$), DOPAC, HAV and 5-HT ($P<0.05$) in both transplantation groups were significantly increased, and there was no significant difference between

exosome-T group and exosome-LV group (P>0.05) (Fig. 2f). The molecular structure of each analyte is shown in the figure (Fig. 2e).

Exosome reduced the damage and apoptosis of DA neuron in the substantia nigra of PD model rats

To observe the protective effect of exosome on DA neurons of SN in PD model rats, we performed haematoxylin and eosin (HE) and immunohistochemistry staining. HE staining showed that the tissue structure of bilateral SN in control group was clear and orderly, the nucleus of neurons was clear and the morphology was integrated. In 6-OHDA group, the number of neurons were decreased and the soma of the neurons swelled, the nucleus was enlarged. Some neuron soma displayed cell body lysis and their nucleus showed vacuolar. Glial cells numbers were increased and proliferated diffusely or locally. Compared with 6-OHDA-treated rats, the edema of neurons in exosomes-lateral ventricle and exosomes-tail vein groups were light. Furthermore, and the glial cell numbers were significantly lesser in exosomes-lateral ventricle and exosomes-tail vein groups than 6-OHDA-treated rats (Fig. 3a). TH-positive immunoreactivity was used as a marker for dopaminergic neurons in the striatum (Fig. 3b). 6-OHDA treatment decreased TH neurons in SN on the damaged side while exosomes-lateral ventricle and exosomes-tail vein significantly recovered the TH neurons (P<0.001) (Fig. 3c).

To further determine the effect of exosome on DA neurons in PD model, TH and TUNEL double-labeled immunofluorescence staining was used to detect the apoptosis of TH neurons. TH and TNEL double positive cells were significantly increased in 6-OHDA-treated rats and decreased in exosomes-LV and exosomes -T groups (both P<0.001) (Fig. 3d and e). These data suggested exosomes reduce apoptosis of DA neurons induced by 6-OHDA. TH and TUNEL double-labeled neurons did not significant difference between exosomes-lateral ventricle group and exosomes-tail vein groups.

Exosome reduced the activation of microglia in substantia nigra of PD model rats

The effect of exosome on microglia activation in lesioned SN was determined by TH and Iba-1 immunofluorescent double staining. We found that microglia in control group with positive Iba-1 expression had long and thin processes, while the expression of Iba-1 increased, and the processes became shorter and thicker in 6-OHDA group. Compared with 6-OHDA group, morphology of microglia in exosome-LV group and exosome-T groups displayed more thinner branches, but the number of microglia had no significant change (Fig. 4a). In addition, the expressions of Iba-1 in exosomes-lateral ventricle group and exosomes-tail vein groups were decreased significantly (P<0.001) (Fig. 4b). These data suggest that exosome inhibited the activation of microglia.

Exosome can be taken by BV2 cells and attenuated the damage of SH-SY5Y cell viability induced by LPS and BV2 activation

To detect whether exosome has a protective effect on injured neurons in vitro, the uptake of exosome by BV2 cells was observed by confocal microscope. Exosome were taken in a small amount by normal BV2 cells at 1h and in large amount at 3h and later (Fig. 5a, left). Exosome was also taken by BV2 after drug

intervention at 24h (Fig. 5a, middle) and entered the interior of the cells (Fig. 5a, middle). Furthermore, confocal microscope 2.5D and 3D scanning showed that exosome entered the BV2 nucleus at 3h (Fig. 5a, right).

To make neuroinflammatory cell model in vitro, first, LPS/ATP were added to BV2 and SH-SY5Y cells, respectively, and cell viability was assessed by CCK8 (Fig. 5b). The supernatant of BV2 induced by LPS/ATP was added into cultured SH-SY5Y cells and the cell viability was detected again (Fig. 5b). The viability of SH-SY5Y (Fig. 5c, up) and BV2 (Fig. 5c, bottom) cells treated with LPS at different concentrations did not decrease significantly, while the viability decreased when added with 5mM ATP, but cell viability value were all >50%. Then, with 1μg/ml LPS+ATP on BV2 cells at different times, the supernatant significantly reduced the viability of SH-SY5Y cells, and the cell viability was reduced to 50% for 3h (Fig. 5d), and 1μg/ml LPS+ATP for 3h was chosen for the vitro model.

To assess the protective effect of exosome on neuroinflammatory cell model, first, the time-concentration curve of exosome acting on BV2 was made. Exosomes at a concentration of 0 to 100 μg/ml didn't affect the cell variability of BV2 for 48h (Fig. 5e), while exosome pretreatment significantly increased the viability of SH-SY5Y cells treated by LPS/ATP-BV2 supernatant from 50 μg/ml to 100 μg/ml (P<0.05). These data suggested that exosome protected neurons by inhibiting the activation of LPS/ATP-induced microglia. Meanwhile, results showed that there was no significant difference between 75 and 100 μg/ml groups (P>0.05). Thus, 75 μg/ml was selected for the subsequent experiments (Fig. 5f).

Exosomes inhibited pyroptosis derived from the induction of LPS/ATP to BV2

To further observe the effect of exosome on BV2 pyroptosis, ELISA, scanning electron microscope and Western blot was used. ELISA results suggested that the secretions of IL-1β and IL-18 in BV2 cell supernatant treated with LPS+ATP were significantly increased, while in exosome group were significantly decreased than in LPS+ATP group (both P<0.001) (Fig. 6a).

The results of scanning electron microscope suggested that the cell morphology in control group was normal and the cell contour was clear. In LPS+ATP group, the cell morphology was irregular, swollen and enlarged, and cells were attached to the climbing films, and there were vesicular substances caused by cytoplasmic overflow. In exosome-treated group, vesicular substances decreased and cell morphology recovered (Fig. 6b).

Western blot results suggested that compared with LPS+ATP group, the bands gray values of related proteins of TLR4-NF-κB pathway, NLRP3-ASC-Caspase 1-NEK7, and caspase-11 mediated pyroptosis pathway as well as HMGB1 in exosomes group were all significantly decreased (P<0.05). These results suggested that exosome inhibited pyroptosis of LPS+ATP-induced BV2 cells. (Fig. 6c)

MiRNA sequencing, protein spectrum analysis and bioinformatics analysis of exosome

To further clarify whether the mechanism of exosome on inhibiting pyroptosis is related to the contained miRNA and protein, high-throughput sequencing of miRNA, mass spectrometry sequencing of protein

carried by LC-MS/MS were performed. We found that 616 miRNA, 14235 target genes and 667 proteins were obtained from exosome. To find the connection between exosome and PD, the database that contained PD pathogenic targets were firstly screened, and the differential genes of cingulum gyrus tissue in GSE110716 (n=16), midbrain-induced pluripotent stem cells in GSE110719 (n=26) between PD patients and the control group were screened. Then these screened genes were intersected with the exosome Top100 genes.

To analyze the functions and related pathways of exosome miRNA, protein and intersected genes with PD, bioinformatics analysis was performed. The GO annotations of the above gene and proteins all included cellular component (CC), molecular function (MF) and biological process (BP). Fig.7a showed the exosome miRNA. According to the PPI analysis for exosome protein, three subsets were obtained in PPI network (Fig. 7d). For KEGG analysis of top 100 miRNA (Fig. 7b), protein (Fig. 7c), and intersection gene (Fig. 7e), Leukocyte trans-endothelial migration, NF-κB, PI3K-Akt, Toll, NOD receptor, TNF and mTOR receptor signaling pathways were enrichment and related to immunity. miR-125-5p, miR-122-5p, miR-126-3p, miR-199-3p were the most abundant miRNA. In addition to the above miRNAs, miR-423-5p, miR-150-5p, miR-34a-5p were also included in the enrichment pathways.

Discussion

Many drugs have the limited effect on cells in the brain because they cannot cross the BBB effectively. Exosomes not only exist in a variety of body fluids[10] and cells and contain various biological information[11], but also have small particle size without immunogenicity, which is more advantageous for intercellular communication. Although studies have shown that intravenous injection of exosomes was absorbed by liver, spleen, lung[12], pancreas and gastrointestinal tract[13] to varying degrees, it presented homing ability and targeting to the damaged area[14], and carried α-Synuclein siRNA[15], shRNA[16], DA and catalase[17] to PD cerebral targeting cells, therefore it became an invisible nanocarrier of PD drugs. The exosome extracted from MSCs survive longer, have lower immunogenicity, and contain the effective components of stem cells, and are more advantageous than exosome derived from other cell sources and stem cell therapy alone.

It has been shown that hucMSCs are able to differentiate into DA cells[18, 19], and strongly inhibit inflammation[20]. This study found a therapeutic effect of hucMSCs- exosomes on PD model rats. Firstly, hucMSCs were obtained by primary culture, and the morphology, growth and three direction differentiation met the criterion of MSCs[21]. Then exosome was extracted from the cell supernatant, and identified as exosome by the morphology, particle size and surface specific antigen assay. In order to better observe the ability of exosome to penetrate BBB and the therapeutic effect on PD, the classic catecholamine neurotoxin 6-OHDA was selected to establish the PD model. Exosome was labeled with PKH26 and injected into the caudal vein and lateral ventricle. Then exosomes reached the damaged substantia nigra of PD rats and were ingested by DA neuron in the SN. These observations suggested that exosome penetrated BBB and aggregated to the damage area. Meanwhile, exosome was able to

improve behavior, reduce neuronal damage and apoptosis, increase striatal DA and the metabolites. The therapeutic effects of both transplantation methods were nearly the same, which proved that the intravenous injection of exosome had the same targeting and utilization as the lateral ventricular injection.

The homeostatic imbalance of neuron-glial network and the activation or reactive gliosis of glial cells[22] are key factors of the occurrence and development of PD. Microglia are macrophages in the neuroectoderm as well as the cerebral immune cells, and the expression in the SN is higher than that in other cerebral regions[23]. The increase of the inflammatory factors[24], such as cyclooxygenase 2 (COX2), prostaglandins (PGs), tumor necrosis factor α (TNF-α), interleukin-3(IL-13), interferon γ (IFN-γ), and activation of microglia play important role in the pathology of PD. Thus, the nonsteroidal anti-inflammatory drug ibuprofen[25], as well minocycline[26] and dexamethasone[27] inhibit microglia activation, suggesting that neuroinflammation is correlated to PD. To determine the anti-inflammatory mechanism of exosome in PD, we first found that exosome was taken by microglia. In PD model group, the microglia labeled by Iba-1 was transformed from ramified to activation, and number of microglia was increased. However, the morphology of the microglia recovered, and the number decreased in exosome-treated group, suggesting that exosome protects neurons by inhibiting the activation of microglia. We found that adding exosomes into normal BV2 cells did not significantly change the viability of BV2 cells, whereas administration of exosomes in 6-OHDA-induced PD mice recovered microglia function as indicated by increasing thin branches and decrease microglia cell numbers. These data suggest that exosomes does not affect normal BV2 cells but recovery activated microglia. We also used an in vitro model to determine the mechanisms involved in the inhibition of neuroinflammation induced by microglia, microglia cell line BV2 was treated by LPS/ATP, and applied supernatant to human neuroblastoma SH-SY5Y with DA-β-hydroxylase activity, and prepared the classic neuroinflammatory model in vitro. We found that the exosome pretreatment for BV2 cells significantly reduced the secretion of IL-18/IL-1B in supernatant and thereby protected SH-SY5Y cells.

Pyroptosis, a newly discovered programmed death of inflammatory cells, has been reported in animals[28] and cell models of PD[29, 30]. TLR4-NF-κB is activated by the first signal damage-associated molecular patterns (DAMPs), pathogen-associated molecular patterns (PAMPs, e.g., LPS), and mediates the expression of IL-1β, IL-18, caspase-1 precursors and NLRP3. Under the action of second signal K^+ efflux and ATP, NLRP3 assembles with ASC and pro-caspase-1 into an inflammasome, which binds to NIMA-related kinase 7 (Nek7). Subsequently, the caspase-1 or caspase-11 is directly activated by LPS, cleaves Gasdermin D to form holes, through which the activated IL-1β and IL-18 release into the extracellular compartment[31]. Together with high-mobility group box 1 (HMGB1)[32], these inflammatory cytokines induce and accelerate the pyroptosis (Fig. 8).

Exosome derived from different stem cells can improve myocardial function[33], intervertebral disc degeneration[34], acute liver damage, oxygen and glucose deprivation[35, 36], and ischemic damage[8] by inhibiting NLRP3 inflammasome or pyroptosis. In the in vitro neuroinflammatory model in this study, by

using scanning electron microscope we found that LPS/ATP-activated BV2 cells had obvious cytoplasmic overflow and the characteristics of pyroptosis, while exosome treatment reduced cell membrane pores and cytoplasmic overflow, and restored the morphology of pyroptosis cells. In addition, exosome reduced the protein expressions of TLR4-NF-κB, NEK7-NLPR3 inflammasome-caspase-1 and caspase-11 mediated pyroptosis pathway and the inflammatory factors, suggesting that exosome inhibits the occurrence of pyroptosis in microglia.

Many studies suggested that exosome exert its action through its own miRNA. In order to further explore miRNA or upstream pathway of exosome, we used miRNA and protein sequencing followed by the bioinformatics analysis of the intersection of exosome and PD target genes, we found that exosomes were involved in a variety of biological activities, including NF-κB, PI3K/Akt, mTOR, and many immune-related signal pathways. PI3K/Akt signal pathway activates both NF-κB and its downstream pathway and inhibited autophagy by PI3K/Akt/mTOR. Autophagy, an intracellular catabolic process, decomposed and phagocytized the over-activated NLRP3 inflammasome. The damaged function of autophagy led to the accumulation of NLRP3 inflammasome and accelerated the progress of pyroptosis[37, 38]. Among the miRNA, miRNA-122/125/126/199 were highly expressed and it was confirmed that they were involved in autophagy[39] and NF-κB pathway activation[40, 41, 42] in other diseases. It is speculated that these miRNAs and inhibit the generation of downstream NF-κB/NLRP3 inflammasome through PI3K/Akt pathway, and eliminate the excess NLRP3 inflammasome by accelerating autophagy and therefore inhibit the occurrence of pyroptosis. The precise mechanism needs to be further explored. In this study, we did not measure the expression of miRNAs including miR-125-5p, miR-122-5p, miR-126-3p, miR-199-3p in the brain after hucMSCs exosomes treatment. The TPM values of miR-125-5p, miR-122-5p, and miR-126-3p were ranked as 1, 2, and 8 among all measured miRNAs, respectively. The TPM-corrected value of miR-199-3p was ranked as 10. We will determine the responses of BV2 and SH-SY5Y cells to overexpression of miRNAs including miR-125-5p, miR-122-5p, miR-126-3p, and miR-199-3p in our future studies.

Materials And Methods

Cell culture and assay

The outer membrane, artery and vein of sterile umbilical cord of neonatus without ethical disputes were peeled off under aseptic conditions, then Watson's jelly was obtained and cut into 1cm^2 pieces, and cultured in serum-free mesenchymal stem cell complete medium at 37℃ and 5% CO_2 incubator for primary culture. The third-generation cells and supernatants were used in the following experiments.

The cell morphology was observed by optical microscope. HucMSCs were seeded on 12-well culture plate, and 3 wells were taken at a fixed time daily from the second day. The cells were stained with trypan blue and counted for 7 consecutive days. The cell growth curve was drawn and its proliferation ability was detected. HucMSCs were digested and centrifuged, suspended in PBS, and CD90 FITC, CD 105PE, CD73APC, CD34 PE, CD45APC, HLA-DR FITC (BD Biosciences®, Sparks, MD, USA) were added respectively, and the surface specific proteins were assayed by flow cytometry (Beckman Coulter, Inc.,

USA). The inductive differentiation medium was added for 3-4 weeks. The oil red O staining was used to stain the lipid droplets, alizarin red was used to stain the calcium nodules, and alisin blue was used to stain the acid mucopolysaccharide in the cartilage tissue. The differentiations into adipogenesis, osteogenesis and chondrogenesis were observed by optical microscope. SH-SY5Y and BV2 cell lines (China Center for Type Culture Collection, CCTCC) were cultured in the incubator with DMEM/F12 containing 10% fetal bovine serum at 37℃ with 5% CO2.

Purification, assay and labeling of exosome

The culture supernatant of hucMSCs was collected and ultrahigh speed differential centrifugation Sorvall™WX+, Thermo Scientific™, USA was used to extract[5] exosome. The extracellular vesicles were separated from the supernatant of medium 3-5 day after the 3rd passage of primary cultured hucMSCs. For the identification[9], exosome was negatively stained with 2% uranyl acetate and the morphology was observed with transmission electron microscope (H-7650, Hitachi, Tokyo, Japan) after drying. PBS was used to dilute exosome to 1×10^7 particles/ml–1×10^9 particles/ml, nanoparticle potentiometric titration and particle size analyzer (ZetaView PMX 110, Particle Metrix Meerbusch, Germany) and 405nm emission light were used to assay the size and quantity of particles. Western blot was used to assay the surface specific proteins of exosome. Exosome were stained according to PKH26 kit instructions. Exosome suspended with staining solution were centrifuged at 4℃, 120000×g for 100 min, then the supernatant was discarded and the labeled exosome were obtained.

Experimental animals

SPF closed colony SD rat, weighing 200-220g, male and female (Hebei In vivo Biotechnology Co., Ltd., license No. SCXK (Ji) 2019-003). Raised in a specific pathogen-free environment, the room temperature was 22±2℃, the humidity was 45-50%, and the light/dark cycle was 12h. All the animal experiments were conducted with the approval of the Institutional Animal Care and Use Committee at the Hebei Medical University and adhered to the guidelines set forth by the National Research Council's Guide for the Care and Use of Laboratory Animals. All methods and data are reported in accordance with ARRIVE guidelines (https://arriveguidelines.org) and recommendations.

Preparation, grouping and behavioral evaluation of PD animal model

PD models were prepared by using a rat brain stereotactic instrument (Neurostar, Tubingen, Germany). Rats were anesthetized with 2% isoflurane, and 2μl 6-OHDA (4μg/μl, soluble in sterile normal saline containing 0.2% ascorbic acid, Sigma, USA) was injected into the right substantia nigra (SNc) (AP –4.4mm, ML +1.2mm, DV +7.8mm) and ventral tegmental area (VTA) (AP –4.8mm, ML +1.0mm, DV +7.8mm) respectively. The control group was injected with the same amount of normal saline containing 0.2% ascorbic acid. On the 21D after operation, Apomorphine (APO, 0.5mg/kg, Sigma, USA) was injected intraperitoneally. Rats with an average speed greater than 7R/min were regarded as the successful model.

The successful modeling rats were randomly divided into model group (6-OHDA), tail vein group and lateral ventricle group. Rats in exosome-tail vein group were injected with 1ml normal saline with 100 μg exosomes, once a day for 14 consecutive days via the tail vein. Rats in the exosome-lateral ventricle group were injected with 10μl normal saline with 100μg exosome in the right lateral ventricle (AP-1.5mm, ML+1.5mm, DV+3.8mm) by using the rat brain stereotactic instrument. The model group was not intervened. APO was injected intraperitoneally into the rats of three groups and control group at 2W, 4W, 6W and 8W after transplantation to induce rotation, then the rotational number per minute was observed and recorded.

High performance liquid chromatography-mass spectrometry (HPLC-MS)

DA, 5-hydroxytryptamine (5-HT) and their metabolites in rat striatum of each group were detected by Ultimate3000 RS chromatograph (Thermo Fisher Scientific, USA) and Q Exactive high resolution mass spectrometer (Thermo Fisher Scientific, USA). The electrospray voltage of mass spectrometry ion source was 3.2kV, the positive and negative ions were scanned alternatively, and the collision gas was high-purity argon, the sheath gas was nitrogen, 40Arb. The chromatographic column was Waters T3, the aqueous phase was 0.1‰ formic acid-water solution, the organic phase was 0.1% formic acid acetonitrile, and the injection volume was 5.00μL. The standards were added to make the standard curve, and the sample was assayed after the treatment with methanol containing 0.1% formic acid.

Haematoxylin and eosin (H&E) staining

Fresh cerebral tissue was fixed with paraformaldehyde, gradient ethanol dehydrated and embedded in paraffin, cut into 4μm slices, dewaxed to water with xylene and ethanol successively, then hematoxylin and eosin were added, stained for 5min respectively, rinsed with running water, went through dehydration and transparent with anhydrous ethanol and xylene, sealed with neutral gum, then the image acquisition was performed with optical microscope.

Immunohistochemistry

The sections were dewaxed to water, afterwards the antigen was repaired with citrate buffer, the endogenous peroxidase was removed with 3% hydrogen peroxide solution, sealed with 3% BSA, added with TH primary antibody (dilution 1:1000, ab112, abcam, Cambridge, UK) overnight at 4℃, and incubated with horseradish peroxidase-labeled secondary antibody (dilution 1:200, GB23303, Servicebio) for 30min at 37℃, 3,3'-diaminobenzidine (DAB) was used as chromogenic agent. Counterstained with hematoxylin for 1min, dehydrated, made to be transparent and sealed. The steps were the same as above and the image acquisition was performed with optical microscope.

Immunofluorescence

In order to observe the colocalization of PKH26 and TH or Iba-1, fresh rat cerebral tissue was taken and prepared for frozen sections (8μm in thickness), TH and Iba-1 (dilution 1:1000, 019-19741, Wako, Japan) primary antibody, fluorescent secondary antibody and DAPI for nucleus staining were used respectively.

In order to observe the expression of Iba-1 in substantia nigra, TH/Iba-1 homologous double label was made. After adding TH primary antibody and secondary antibody, FITC-TSA was added and incubated in the dark for 10min. After antigen repairment, Iba-1 primary antibody and fluorescent secondary antibody containing CY3 (1:250, GB21403, Servicebio) were added and incubated in the dark for 50min, and DAPI were used to stain nucleus; In order to observe the apoptosis of substantia nigra neurons, PBS containing 0.1% triton was used to rupture the membrane, TUNEL reaction solution was added and incubated at 37℃ for 2h, BSA was used for seal at room temperature for 30min, then TH primary antibody and fluorescent secondary antibody were added, and DAPI were used to stain nucleus. The image acquisition was performed with fluorescence microscope.

In vitro uptake of exosome

PKH26-labeled exosome was suspended in the culture medium, and co-cultured with normally cultured BV2 cells and BV2 cells with LPS/ATP intervention for different time, fixed with paraformaldehyde, sealed with the sealing agent containing DAPI, and performed the image acquisition with confocal microscope.

Cell viability assay (CCK8)

The cells were seeded at 96-well culture plate, and set blank wells (culture medium), control wells (normal cells) and experimental wells. Discarded the supernatant after drug or Exos intervention and added 100μl fresh medium containing 10μl CCK8 to each well, then cultured for 2.5h, and detected the absorbance value by microplate reader at 450nm. Calculated cell viability based on the formula: cell viability(%)=(OD experimental well-OD blank well)/(OD control well-OD blank well)×100%. Three duplicated wells were set in each group, and repeated the experiment for three times.

Scanning electron microscope

The cell climbing films were fixed in 2.5% glutaraldehyde for 2-4h, rinsed with phosphate solution for 3 times, and fixed at 1% osmic acid at 4℃ for 2h. After rinsing with double-distilled water for 3 times, gradient ethanol dehydrated, isoamyl acetate replaced, dried with drying apparatus in critical point. After coating with ion sputter coater, performed the image acquisition with scanning electron microscope (Hitachi Regulus 8100, Japan).

ELISA

The cell supernatant was assayed by ELISA. Added 10 μl standards and 10 μl samples to be tested into the wells of microplate respectively. According to the instructions of the kit, added 50μl IL-1β and IL-18 antibodies and 100μl horseradish peroxidase-labeled streptavidin to each well. 100 μl TMB was used as chromogenic agent, assayed the absorbance value at the wavelength of 450 nm and 570 nm, the correction value = OD_{450nm}-OD_{570nm}.

Western blot

Cells were precipitated and added with cell lysate on ice for 30min, 12000g, centrifuged at 4℃ for 20min to extract cell protein, and assayed the concentration by BCA method. Added protein loading buffer at 97℃ for 5min to denaturate protein completely, then performed SDS-PAGE electrophoresis and transmembrane, and sealed with 5% skimmed milk at 37℃ for 1h. Added the primary antibody: TSG101 (sc-13611, Santa Cruz, CA, USA) diluted to 1:500, GAPDH (10494-1-AP, Proteintech, USA) diluted to 1:10000, and other antibodies CD63, Alix, Calnexin (sc-5275, sc-53540, 10427-2-AP, Promega, Madison, WI), NEK7 (GB112643, Servicebio, China), NLRP3 (ab263899, abcam, UK), TLR4 (gb11519, Servicebio, China), NF-κB (GB11997, Servicebio, China), p-NF-κB (ab16502, abcam, UK), antibodies of pyroptosis pathway (98303, CST, USA), diluted to 1:1000, and overnight at 4℃, rinsed by TBST, secondary antibody incubation at 37℃ for 1h, photographed with ECL developer (Millipore, USA), and analyzed the gray value by Image J software (NIH).

miRNA high throughput sequencing of hucMSCs-exosome

The total RNA of Exosomes was extracted and purified. A small RNAs library was constructed by using SMARTer Stranded Total RNA-Seq kit (Takara Bio USA, Inc.), and the library was sequenced by using Illumina Hiseq2500 high-throughput sequencer. Sequence alignment was performed between the clean reads and Silva, GtRNAdb, Rfam, Repbase, human genome (GRCh38), and miRBase (v22) database respectively by using Bowtie software to obtain the known miRNA, then predicted the target gene by miRanda and RNAhybrid. The threshold to define miRNA candidates in HuMSC exosomes were $p<0.05$ FC>1.5, and averaged TPM>10.

Protein spectrum sequencing of hucMSCs-Exos

The label-free protein spectrum sequencing of Exos protease peptides was performed by using liquid-chromatography-tandem mass spectrometry (LC-MS/MS) method (Q Extractive HF-X mass spectrometer, Thermo Fisher, USA). Searched for the original data detected by MS in UniProt database. By using Proteome Discoverer software version 2.2, identified and corrected the peptide signals in LC-MS data, and performed the quantitation and integration, and obtained all proteomic data.

Bioinformatics analysis

Gene ontology (GO) functional annotation was performed by using David online database, and KOBAS v2.0 was used for enrichment analysis of Kyoto Encyclopedia of Genes and Genomes (KEGG) signal pathway. The protein-protein-interaction (PPI) network of top100 protein was constructed in the string database, and obtained the subset by using MCODEC plugin of Cytoscape3.6.1. Based on GEO DataSets database, set Parkinson's disease as the keywords, selected "Homo sapiens" to screen targets, then obtained the target gene intersection with Exos, and analyzed the possible targets of exosome treatment of PD.

Statistical analysis

SPSS 20.0 software was used for results analysis. The random number method was used for grouping. One way ANOVA was used for analysis. LSD was used for pairwise comparison between groups. All data were expressed by mean values ± SD, and $P<0.05$ was considered statistically significant.

Declarations

Acknowledgements

This work was supported by grants from National Natural Science Foundation of Hebei Province (grant numbers: 18967728D, H2021423063); Youth top talent project of colleges and universities in Hebei Province (grant numbers: BJ2021033); National Natural Science Foundation of China (grant numbers: 81873230).

Author Contributions

Z-X.Z, P.G., Y-J.Z., R-Y.W., L-Y.Z., Q-Z.C., W.Z. X-Q.C., H-X.C., S-K.S., L-Q.Z., K.Z., H-J.X., X-Q.C and S.A. designed the study, analyzed and interpreted the data, and drafted the manuscript. Z-X.Z, P.G., Y-J.Z., R-Y.W., L-Y.Z., Q-Z.C., W.Z. X-Q.C., H-X.C., L-Q.Z., K.Z., and S.A. conducted the experiments and analyzed the data. All authors have read and approved the final version of the manuscript.

Data Availability Statement

The original contributions presented in the study are available upon request.

Conflict of interest

The authors declare that they have no conflict of interest.

Ethics Statement

The animal study was reviewed and approved by the Animal Care and Management Committee of Hebei Medical University.

References

1. McGeer, P. L., Itagaki, S., Boyes, B. E., McGeer, E.G. Reactive microglia are positive for HLA-DR in the substantia nigra of Parkinson's and Alzheimer's disease brains. *Neurology* **38,** 1285-1291 (1988).
2. Chung, T. H., et al. Dextran-coated iron oxide nanoparticle-improved therapeutic effects of human mesenchymal stem cells in a mouse model of Parkinson's disease. *Nanoscale* 2018 **10**, 2998-3007 (2018).
3. Weiss, M. L., et al. Human umbilical cord matrix stem cells: preliminary characterization and effect of transplantation in a rodent model of Parkinson's disease. *Stem Cells* **24,** 781-92 (2006).

4. Zhang, B. et al. HucMSC-Exosome Mediated-Wnt4 Signaling Is Required for Cutaneous Wound Healing. *Stem Cells* **33**, 2158-68 (2015).
5. Chen, H. Xu. et al. Exosomes derived from mesenchymal stem cells repair a Parkinson's disease model by inducing autophagy. *Cell Death Dis.* **11**, 288 (2020).
6. Zhang, S. Q. et al. Pretreatment of exosomes derived from hUCMSCs with TNF-α ameliorates acute liver failure by inhibiting the activation of NLRP3 in macrophage. *Life Sci.* **246**, 117401 (2020).
7. Zhang, W., Wang, Y., Kong, Y. C. Exosomes Derived From Mesenchymal Stem Cells Modulate miR-126 to Ameliorate Hyperglycemia-Induced Retinal Inflammation Via Targeting HMGB1. *Invest Ophthalmol Vis Sci.* **60**, 294-303 (2019).
8. Yan, B. et al. Stem cell-derived exosomes prevent pyroptosis and repair ischemic muscle injury through a novel exosome/circHIPK3/ FOXO3a pathway. *Theranostics* **10**, 6728-6742 (2020).
9. Witwer, K. W., Soekmadji, C., Hill, A. F., Wauben, M. H., Buzás, E. I., Vizio, D. D. Updating the MISEV minimal requirements for extracellular vesicle studies: building bridges to reproducibility. *J Extracell Vesicles* **6**, 1396823 (2017).
10. Pan, B. T., Johnstone, R. M. Fate of the transferrin receptor during maturation of sheep reticulocytes in vitro: selective externalization of the receptor. *Cell* **33**, 967-78 (1983).
11. Valadi, H., Ekström, K., Bossios, A., Sjöstrand, M., Lee, J. J., Lötvall, J. O. Exosome-mediated transfer of mRNAs and microRNAs is a novel mechanism of genetic exchange between cells. *Nat Cell Biol.* **9**, 654-9 (2007).
12. Imai, T., Takahashi, Y., Nishikawa, M., Kato, K., Morishita, M. Yamashita, T. Macrophage-dependent clearance of systemically administered B16BL6-derived exosomes from the blood circulation in mice. *J Extracell Vesicles* **4**, 26238 (2015).
13. Wiklander, O. P., Nordin, J. Z., O'Loughlin, A. Gustafsson, Y., Corso, G., Mäger, I. Extracellular vesicle in vivo biodistribution is determined by cell source, route of administration and targeting. *J Extracell Vesicles* **4**, 26316 (2015).
14. Perets, N., Betzer, O., Shapira, R., Brenstein, S., Angel, A., Sadan, T. Golden Exosomes Selectively Target Brain Pathologies in Neurodegenerative and Neurodevelopmental Disorders. *Nano Lett.* **19**, 3422-3431 (2019).
15. Cooper, J. M. et al. Systemic exosomal siRNA delivery reduced alpha-synuclein aggregates in brains of transgenic mice. *Mov Disord.* **29**, 1476-85 (2014).
16. Izco, M. et al. Systemic Exosomal Delivery of shRNA Minicircles Prevents Parkinsonian Pathology. *Mol Ther.* **27**, 2111-2122 (2019).
17. Qu, M. K. et al. Dopamine-loaded blood exosomes targeted to brain for better treatment of Parkinson's disease. *J Control Release* **287**, 156-166 (2018).
18. Datta, I., Mishra, S., Mohanty, L., Pulikkot, S., Joshi, P. G. Neuronal plasticity of human Wharton's jelly mesenchymal stromal cells to the dopaminergic cell type compared with human bone marrow mesenchymal stromal cells. *Cytotherapy* **13**, 918-32 (2011).

19. Meng, X. H., Sun, B., Xue, M. Y., Xu, P., Hu, F. H., Xiao, Z. D. Comparative analysis of microRNA expression in human mesenchymal stem cells from umbilical cord and cord blood. *Genomics* **107**, 124-31. (2016).
20. Bárcia, R. N. et al. What Makes Umbilical Cord Tissue-Derived Mesenchymal Stromal Cells Superior Immunomodulators When Compared to Bone Marrow Derived Mesenchymal Stromal Cells? *Stem Cells Int.* **2015**, 583984 (2015).
21. Dominici, M. et al. Minimal criteria for defining multipotent mesenchymal stromal cells. The International Society for Cellular Therapy position statement. *Cytotherapy* **8**, 315-7 (2006).
22. Balasingam, V. Tejada-Berges, T., Wright, E., Bouckova, R., Yong, V. W. Reactive astrogliosis in the neonatal mouse brain and its modulation by cytokines. *J Neurosci.* **14**, 846-56 (1994).
23. Patel, D. C., Tewari, B. P., Chaunsali, L., Sontheimer, H. Neuron-glia interactions in the pathophysiology of epilepsy. *Nat Rev Neurosci.* **20**, 282-297 (2019).
24. Hirsch, E. C., Hunot, S. Neuroinflammation in Parkinson's disease: a target for neuroprotection? *Lancet Neurol.* **8**, 382-97 (2009).
25. Gao, X., Chen, H. L., Schwarzschild, M. A., Ascherio, A. Use of ibuprofen and risk of Parkinson disease. *Neurology* **76**, 863-9 (2011).
26. Du, Y. et al. Minocycline prevents nigrostriatal dopaminergic neurodegeneration in the MPTP model of Parkinson's disease. *Proc Natl Acad Sci U S A.* **98**, 14669-74 (2001).
27. Tentillier, N. et al. Anti-Inflammatory Modulation of Microglia via CD163-Targeted Glucocorticoids Protects Dopaminergic Neurons in the 6-OHDA Parkinson's Disease Model. *J Neurosci.* **36**, 9375-90 (2016).
28. Zhang, X., Zhang, Y. M., Li, R., Zhu, L. P., Fu, B. Q., Yan, T. H. Salidroside ameliorates Parkinson's disease by inhibiting NLRP3-dependent pyroptosis. *Aging (Albany NY)* **12**, 9405-9426 (2020).
29. Sarkar, S. et al. Mitochondrial impairment in microglia amplifies NLRP3 inflammasome proinflammatory signaling in cell culture and animal models of Parkinson's disease. *NPJ Parkinsons Dis.* **3**, 30 (2017).
30. Li, M. Y. et al. Adrenomedullin alleviates the pyroptosis of Leydig cells by promoting autophagy via the ROS-AMPK-mTOR axis. *Cell Death Dis.* **10**, 489 (2019).
31. Bedoui, S., Herold, M. J., Strasser, A. Emerging connectivity of programmed cell death pathways and its physiological implications. *Nat Rev Mol Cell Biol.* **21,** 678-695 (2020).
32. He, M. Z., Bianchi, M. E., Coleman, T. R., Tracey, K. J., Al-Abed, Y. Exploring the biological functional mechanism of the HMGB1/TLR4/MD-2 complex by surface plasmon resonance. *Mol Med.* **24**, 21. (2018).
33. Singla, D. K., Johnson, T. A., Dargani, Z. T. Exosome Treatment Enhances Anti-Inflammatory M2 Macrophages and Reduces Inflammation-Induced Pyroptosis in Doxorubicin-Induced Cardiomyopathy. *Cells* **8,** 1224 (2019).

34. Zhang, J. W. et al. Mesenchymal stem cells-derived exosomes ameliorate intervertebral disc degeneration through inhibiting pyroptosis. *J Cell Mol Med.* **24,** 11742-11754 (2020).
35. Chen, X. et al. Mesenchymal stem cell-derived exosomes ameliorate intervertebral disc degeneration via anti-oxidant and anti-inflammatory effects. *Free Radic Biol Med.* **143**, 1-15 (2019).
36. Liu, Y. N. et al. AMSC-derived exosomes alleviate lipopolysaccharide/d-galactosamine -induced acute liver failure by miR-17-mediated reduction of TXNIP/NLRP3 inflammasome activation in macrophages. *E Bio Medicine* **36**, 140-150 (2018).
37. Shi, C. S. et al. Activation of autophagy by inflammatory signals limits IL-1beta production by targeting ubiquitinated inflammasomes for destruction. *Nat Immunol.* **13**, 255-63 (2012).
38. Deretic, V., Saitoh, T., Akira, S. Autophagy in infection, inflammation and immunity. *Nat. Rev. Immunol.* **13**, 722-37 (2013).
39. Santovito, D. et al. Autophagy unleashes noncanonical microRNA functions. *Autophagy* **16**, 2294-2296 (2020).
40. Kim, S. W., Ramasamy, K., Bouamar, H., Lin, A. P., Jiang, D. F., Aguiar, R.C. MicroRNAs miR-125a and miR-125b constitutively activate the NF-κB pathway by targeting the tumor necrosis factor alpha-induced protein 3 (TNFAIP3, A20). *Proc Natl Acad Sci U S A.* **109**, 7865-70 (2012).
41. Niu, J. L., Jin, Z.Q., Kim, H., Kolattukudy P. E. MCP-1-induced protein attenuates post-infarct cardiac remodeling and dysfunction through mitigating NF-κB activation and suppressing inflammation-associated microRNA expression. *Basic Res Cardiol.* **110**, 26 (2015).
42. Rivkin, M. et al. Inflammation-Induced Expression and Secretion of MicroRNA 122 Leads to Reduced Blood Levels of Kidney-Derived Erythropoietin and Anemia. *Gastroenterology* **151**, 999-1010 (2016).

Figures

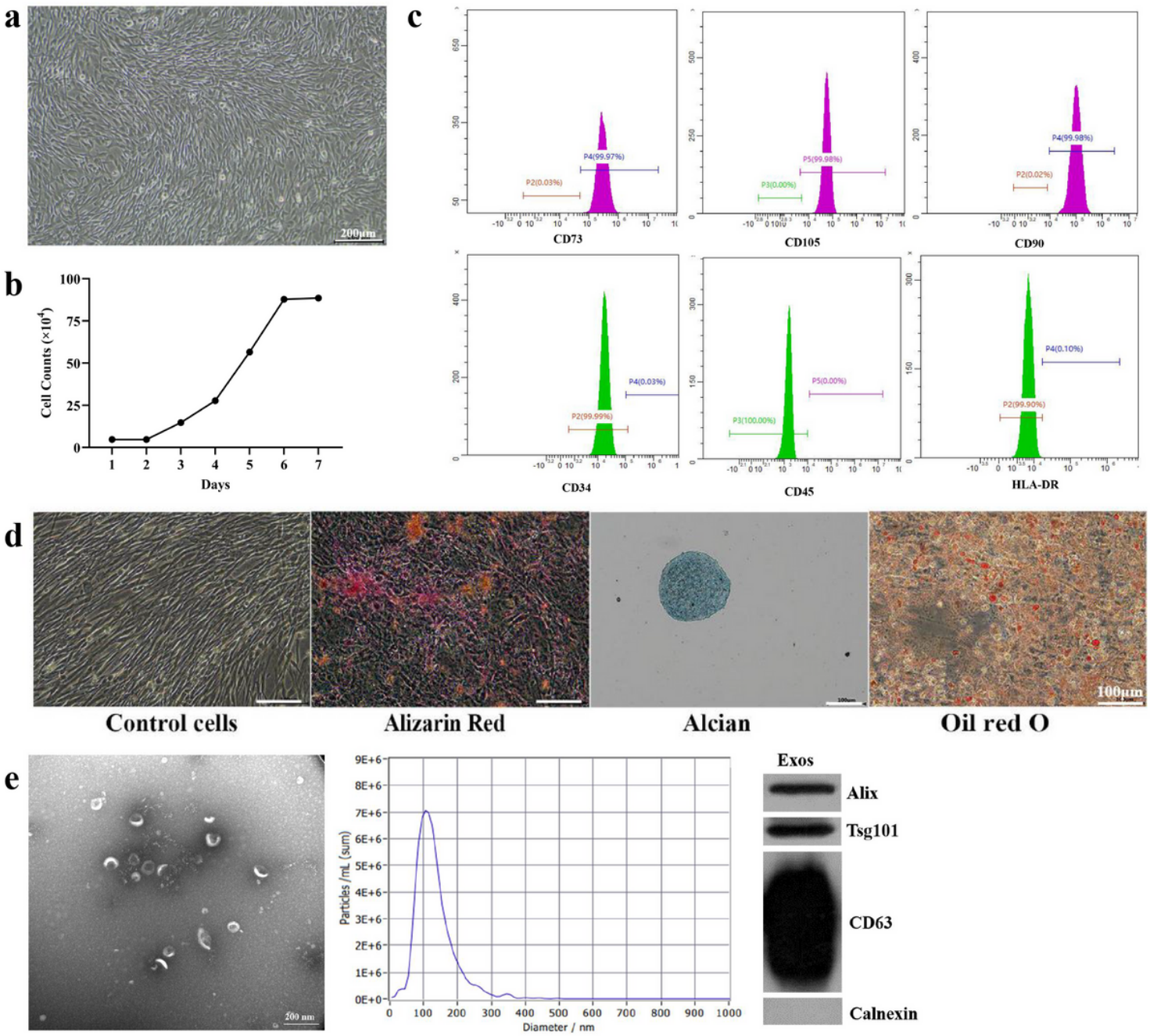

Figure 1

Typical characteristics of hucMSCs and hucMSCs-Exosome. a. Morphology of hucMSCs. **b.** Growth curve of hucMSCs. **c.** The surface antigen of hucMSCs was assayed by flow cytometry. **d.** Three direction differentiation results. **e.** Typical characteristics of Exosome: transmission electron microscope (TEM) image (left), particle size showed by nano-particle size tracking analysis (NTA) (middle), Exosome markers showed by Western blotting (right).

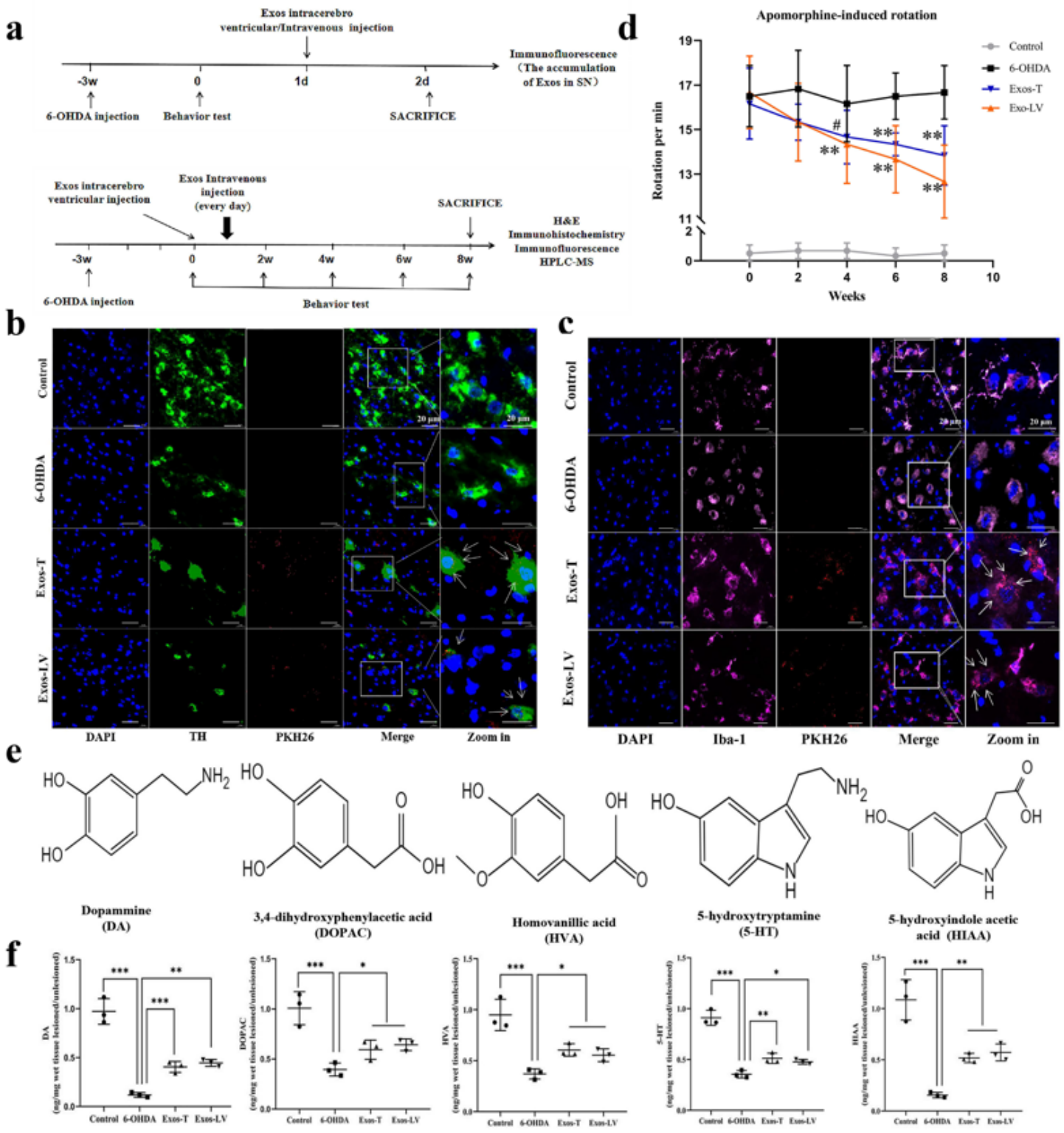

Figure 2

Exosome co-located with DA neuron and microglia in the lesioned substantia nigra, improved the behavior, and increased the contents of DA and the metabolites in lesioned striatum of PD model rats. **a.** The schematic diagram of in vivo experiment. **b.** The colocalization of Exosome (red) and DA neurons (green) with positive TH expression in lesioned substantia nigra. **c.** The colocalization of Exosome (red) and microglia (pink) with positive Iba-1 expression in lesioned substantia nigra. Blue was DAPI-stained

nucleus (n=3). The arrow represents Exosome and the box represents the enlarged area. **d.** The intraperitoneal injection of APO (0.5mg/kg) induced rotation in rats. Induction was performed 21 days after model preparation (before transplantation, i.e. 0W) and 2W, 4W, 6W and 8W after exosome transplantation. Control group: no injection of 6-OHDA and Exosome; 6-OHDA group: injection of 6-OHDA without Exosome Exosome-tail vein group: 6-OHDA+Exosome injected by tail vein; Exosome-lateral ventricle group: 6-OHDA+Exosome injected by lateral ventricle. ** *P*<0.01 *vs* 6-OHDA group before transplantation (0W), # *P*<0.01 *vs* before transplantation (0W) (n=6). **e.** The chemical structure of all analytes. **f.** The levels of metabolites were assayed by HPLC-MS. All data were represented by mean values ± SD. * *P*<0.05, ** *P* <0.01, *** *P*<0.001 (n=3).

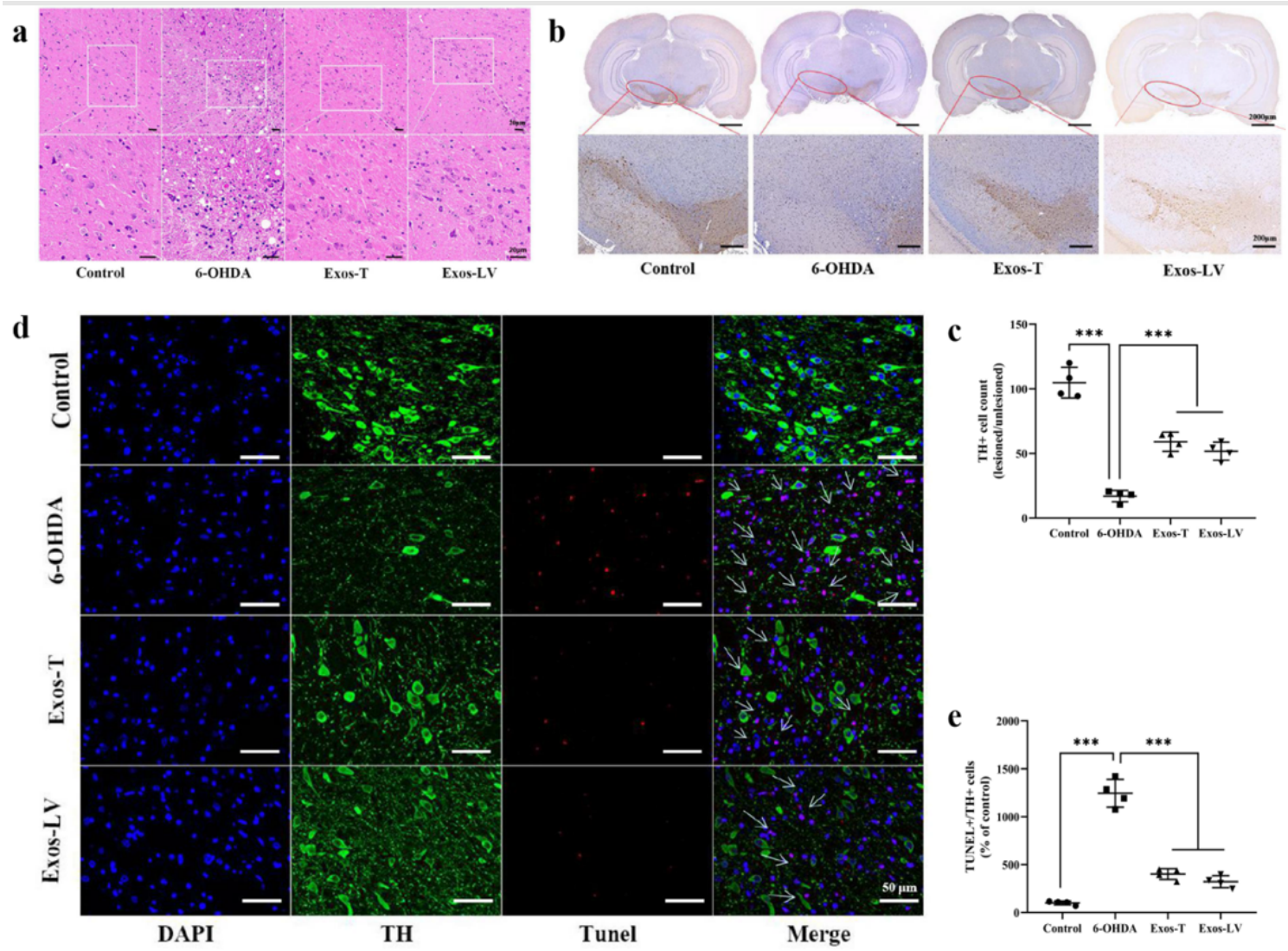

Figure 3

Exosome reduced the damage and apoptosis of DA neuron in the substantia nigra of PD model rats. a. HE staining. **b**. TH immunohistochemical staining of substantia nigra. Embedded and sliced from the head side, the left side was the damaged side and the right side was the undamaged side. **c**. The comparison of bilateral TH expression ratio. **d**. The expressions of TH (green) and TUNEL (red) in neuron

in the substantia nigra. Blue was DAPI-stained nucleus. **e**. The quantitative comparison of TUNEL+/TH+. Arrows indicated the neurons with positive expressions of TUNEL and TH and the circle represents the enlarged area. All data were represented by mean values ± SD. ***P<0.001 (n=4).

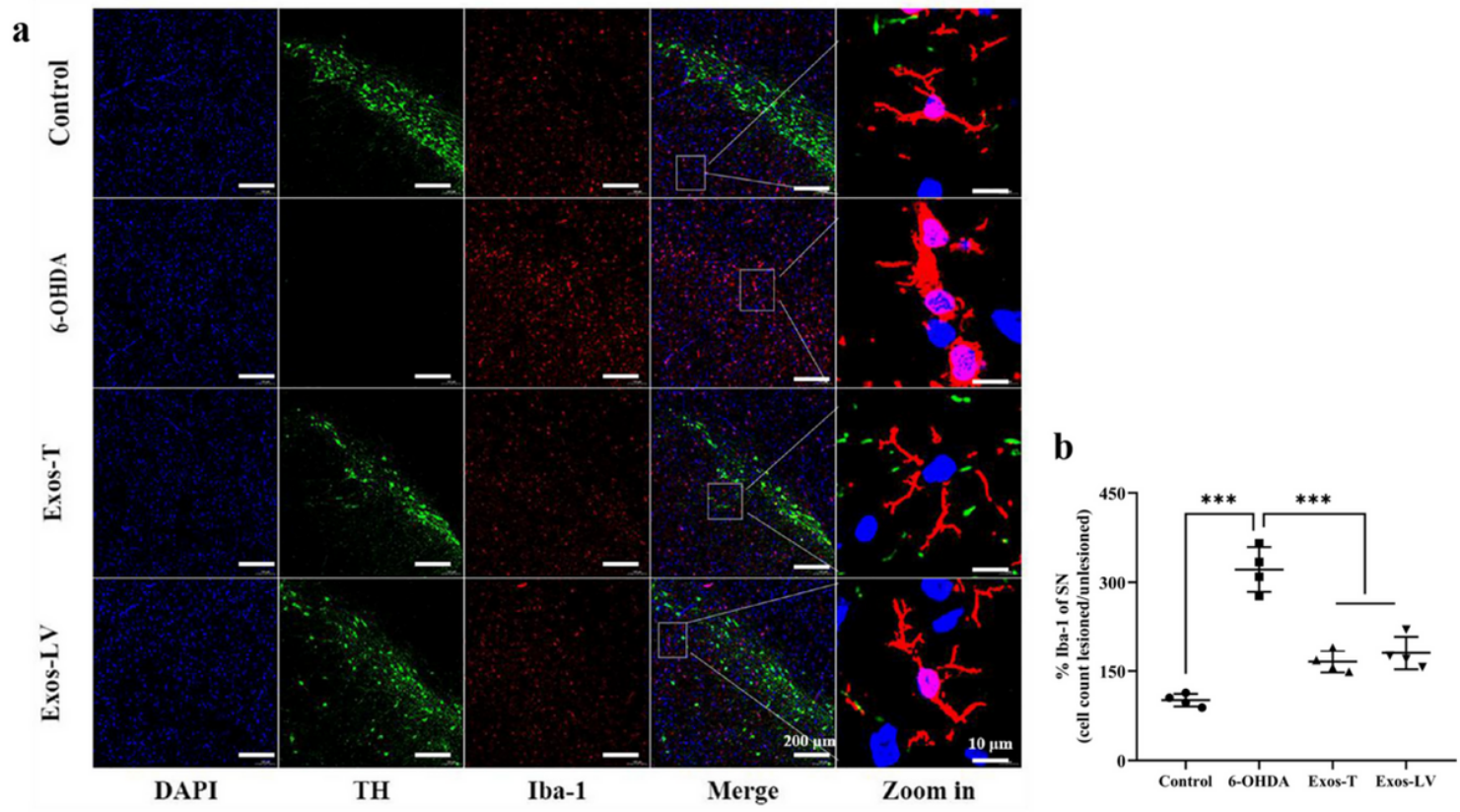

Figure 4

Exosome reduced the activation of microglia in substantia nigra of PD model rats. a. The expressions of Iba-1 (red) in substantia nigra of rats of each group. Blue was DAPI-stained nucleus and green was TH indicating substantia nigra region. **b.** The quantitative comparison of Iba-1. The box represents the enlarged area. All data were represented by mean values ± SD. ***P<0.001 (n=4).

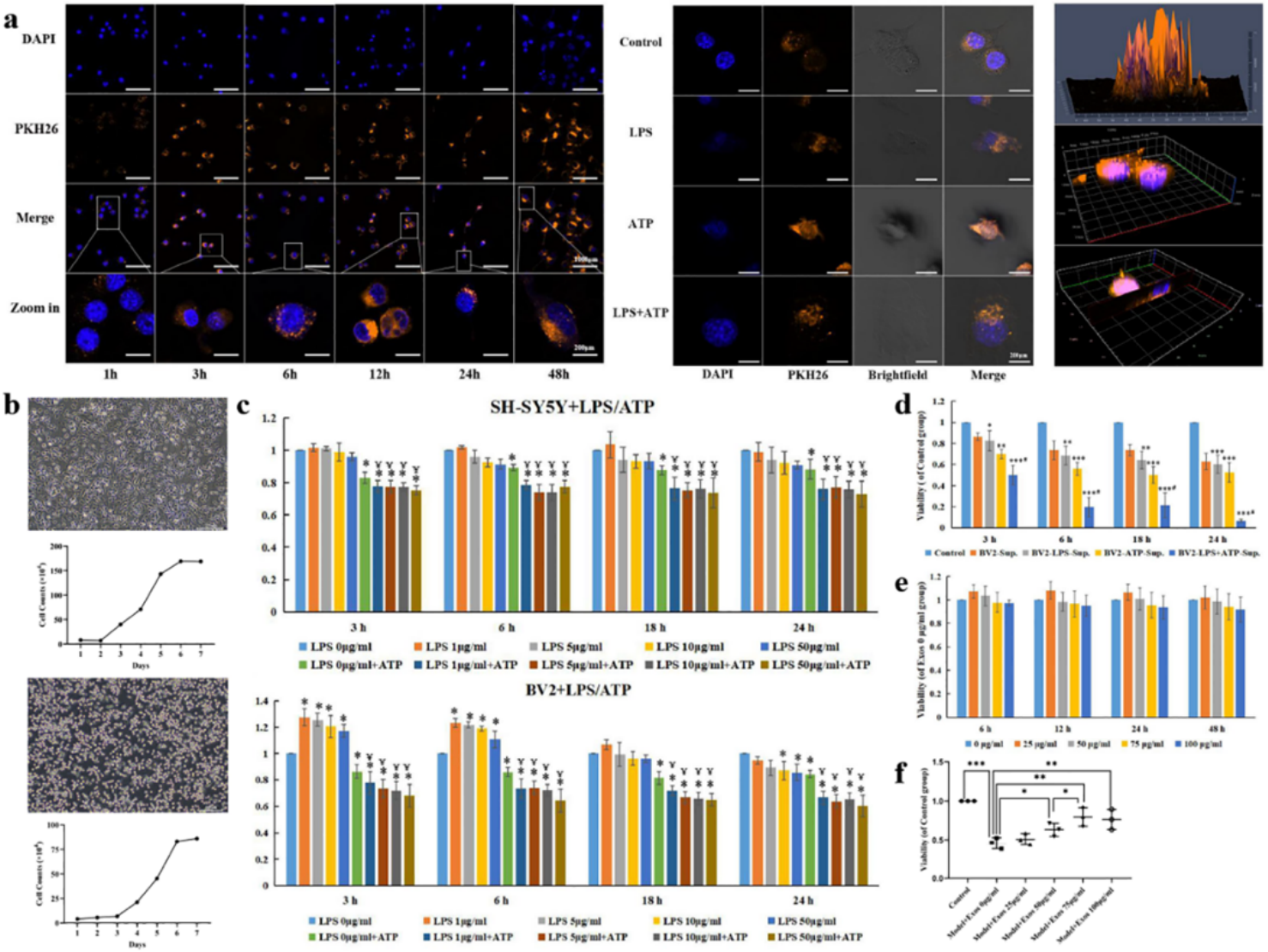

Figure 5

Exosome can be taken by BV2 cells and improved the damage of SH-SY5Y cell viability induced by LPS and BV2 activation. a. Uptake of Exosome by normal BV2 cells at different time (left), by BV2 in case of drug intervention at 24h (middle), and confocal microscope 2.5D (up) and 3D (middle and bottom) scanning of Exosome in normal BV2 cells at 3h (right). Bright field and scanning showed Exosome entered into BV2 cells. Blue was the nucleus and orange was Exosome. The box represents the enlarged area. **b.** Morphology and growth curve of SH-SY5Y (up) and BV2 cells (bottom). **c.** The effect of LPS/ATP on the viability of SH-SY5Y cells (up) and BV2 cells (bottom). **d.** BV2 supernatant treated by LPS+ATP reduced SH-SY5Y cell viability. **e.** The concentration-time curve of Exosome on BV2 cell viability. The cell viability didn't change significantly (P>0.05) from 0 to 100 μg/ml for 6h, 12h, 24h, 48h. **f.** The effect of different concentrations of Exosome for 6h on SH-SY5Y cell viability intervened by supernatant of BV2 cells induced by LPS+ATP. Cell viability was assessed by CCK-8. All data were represented by mean values ± SD. c. *P<0.01 vs LPS 0 group P<0.05 vs LPS 0+ATP group d.f. *P<0.05 **P<0.01, ***P<0.001 vs Control group #P<0.05 vs BV-sup group (n=4).

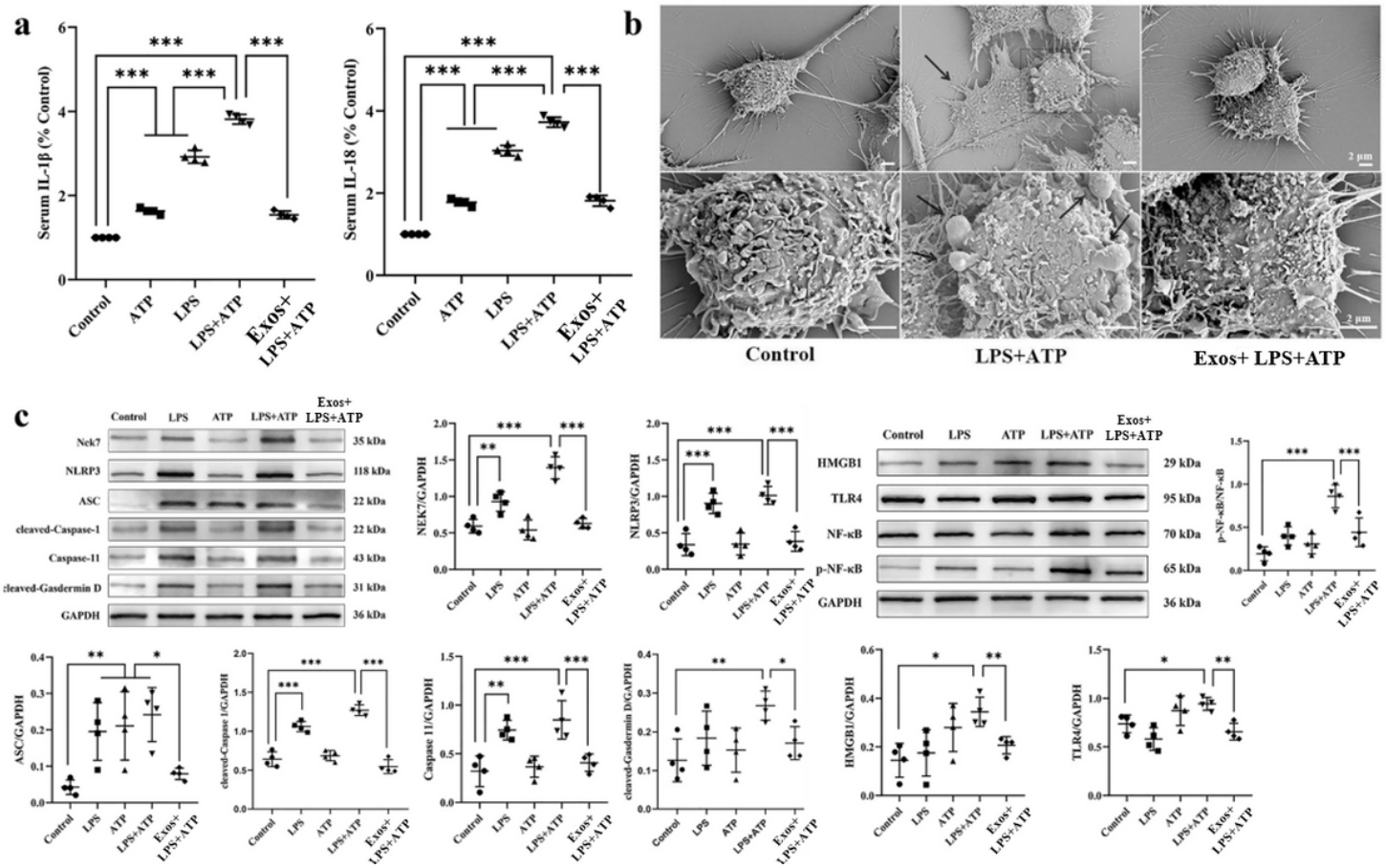

Figure 6

Exosome inhibited pyroptosis derived from the induction of LPS/ATP to BV2. a. The effect of Exosome on IL-1β and IL-18 was assayed by ELISA. **b**. The effect of Exosome on the morphology of BV2 pyroptosis cells was observed by scanning electron microscope. **c**. The effect of Exosome on pyroptosis-related proteins was assayed by Western blot. The arrow pointed to pyroptosis cell. All data were represented by mean values ± SD. **P*<0.05 ***P*<0.01 ****P*<0.001 (n=4).

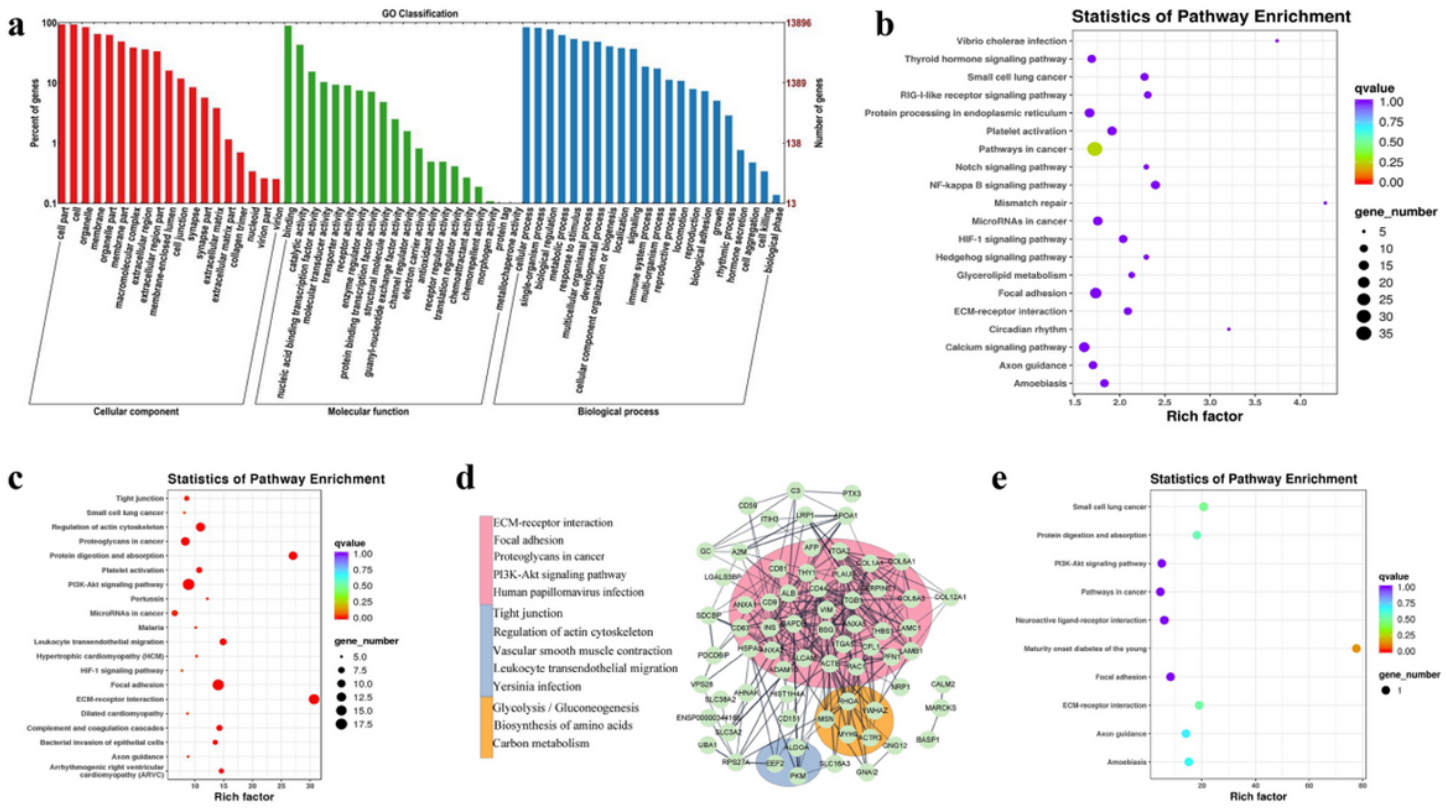

Figure 7

miRNA, Protein spectrum sequencing and Bioinformatics analysis of Exosome. a. GO annotation of miRNA target genes. **b**. The bubble chart of KEGG analysis of Top100 miRNA target genes. **c**. The bubble chart of KEGG analysis of Top100 proteins. **d**. Top100 PPI network, nodes represented proteins, lines represented correlation, different colors represented different subsets, and the left side was the KEGG enrichment analysis result top5 in the subset. **e**. KEGG analysis of intersection gene of Exosome and GSE110716. The color of the bubble represented the Q value and the size represented the gene number.

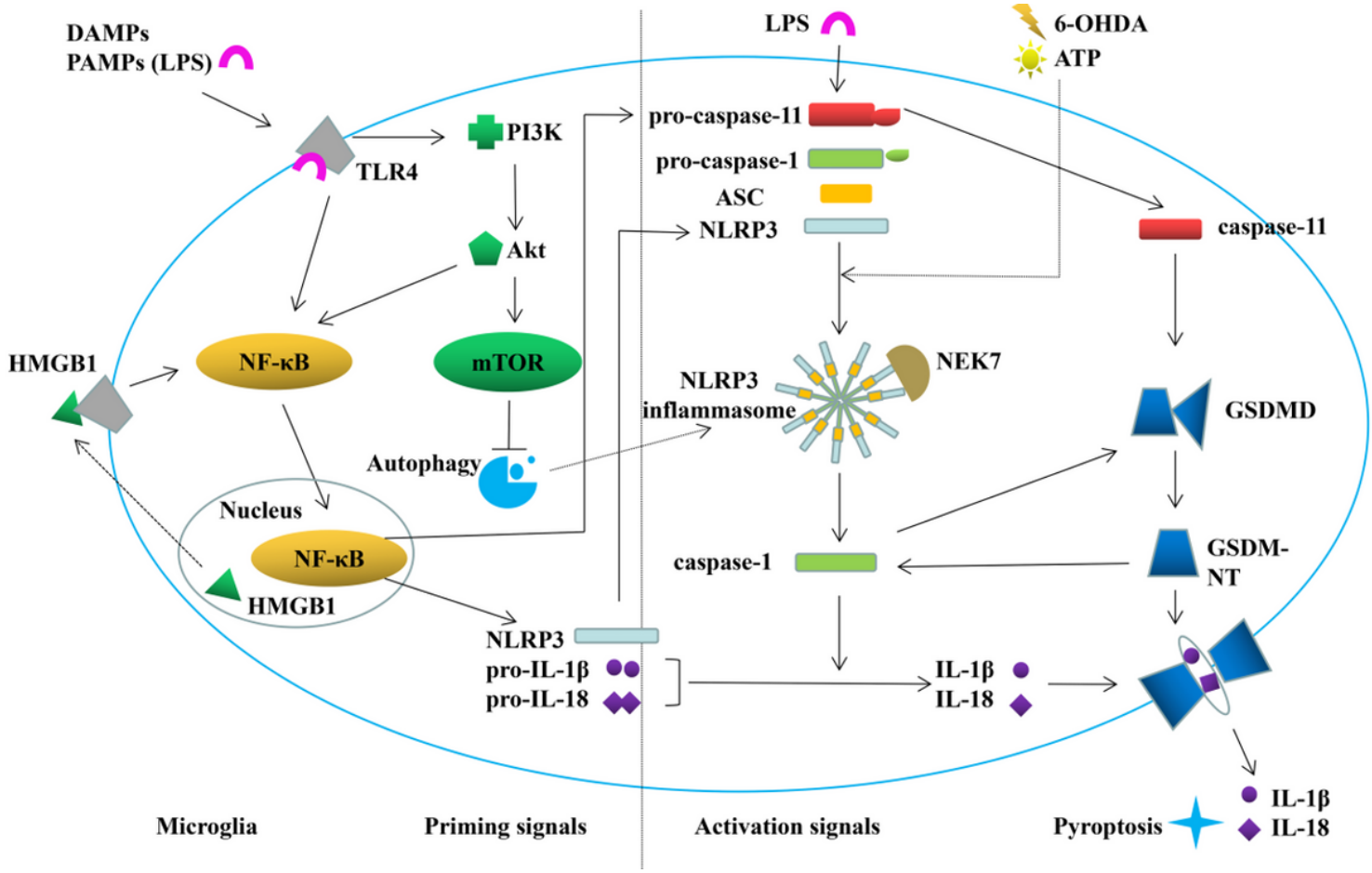

Figure 8

Microglia pyroptosis and the therapeutic mechanism of Exosome in PD

LPS combined with TLR4 and induced pyroptosis by caspase-1 and caspase-11 respectively and also activated the intracellular PI3K/Akt pathway and then activated NF-κB and mTOR, accelerated NLRP3 inflammatory corpuscle aggregation and pyroptosis. hucMSCs-Exosome may inhibit the occurrence and development of pyroptosis by TLR4/NF-κB and PI3K/AKT pathway.